Counter-intuitive results in acousto-elasticity

CrossMark

A.L. Gower [a,*], M. Destrade [a,b], R.W. Ogden [c]

[a] School of Mathematics, Statistics and Applied Mathematics, National University of Ireland Galway, University Road, Galway, Ireland
[b] School of Mechanical & Materials Engineering, University College Dublin, Belfield, Dublin 4, Ireland
[c] School of Mathematics and Statistics, University of Glasgow, Scotland, United Kingdom

HIGHLIGHTS

- We revisit the theory of acousto-elasticity in deformed isotropic solids.
- Intuition suggests that slowest and the fastest waves should travel along the directions of least and greatest stretch.
- We find examples where this is not the case, for body and for surface waves.
- These results complicate accepted protocols for finding the directions of greatest strains.

ARTICLE INFO

ABSTRACT

We present examples of body wave and surface wave propagation in deformed solids where the slowest and the fastest waves do not travel along the directions of least and greatest stretch, respectively. These results run counter to commonly accepted theory, practice, and implementation of the principles of acousto-elasticity in initially isotropic solids. For instance, we find that in nickel and steel the fastest waves are along the direction of greatest compression, not greatest extension (and vice-versa for the slowest waves), as soon as those solids are deformed. Further, we find that when some materials are subject to a small-but-finite deformation, other extrema of wave speeds appear in non-principal directions. Examples include nickel, steel, polystyrene, and a certain hydrogel. The existence of these "oblique", non-principal extremal waves complicates the protocols for the non-destructive determination of the directions of extreme strains.

1. Introduction

The determination of the direction of greatest tension in a deformed solid is one of the main goals of acoustic non-destructive evaluation because, for isotropic solids, this direction coincides with the direction of greatest stress. Consider for instance cutting through a membrane under uniaxial tension: cutting parallel to the direction of the tensile force produces a thin cut, while cutting across produces a gaping cut (see Fig. 1), which can have serious consequences in scaring outcomes after stabbing incidents or surgery. Finding the direction of greatest stress is also important in geophysics, oil prospecting [1] and structural health monitoring and evaluation [2,3].

In this paper, we investigate the propagation of small-amplitude elastic waves in the body (body acoustic waves—BAWs) and on the surface (surface acoustic waves—SAWs) of a deformed solid, and determine the dependence of their speeds on the angle of propagation with respect to the principal directions of pre-strain. It is widely thought that surface waves propagate at their fastest in the direction of greatest stretch and at their slowest in a perpendicular direction, along the direction of least stretch. This view is supported by intuition and often forms the basis of a non-destructive determination of these directions.

---

* Corresponding author. Tel.: +353 91492405.
  E-mail address: arturgower@gmail.com (A.L. Gower).

Fig. 1. Cutting through pig skin: a clamped sample of pig skin is put under tension, after 3 cuts have been performed, parallel (top), oblique (center) and perpendicular (bottom) to the tensile force.

However, the coupling of acoustics and elasticity is a *non-linear phenomenon* even at its lowest order, and it can thus generate counter-intuitive results. The first such result is that for some materials, the fastest wave travels along the direction of greatest compression (and conversely, the slowest wave along the direction of greatest extension). It has been known for some time that a compression in one direction could indeed result in an increase in the speed of a principal wave instead of the intuitively expected decrease, and Hughes and Kelly [4] showed experimentally that body wave speeds increase with hydrostatic pressure for polystyrene (see their Fig. 3); similar experimental results exist for body waves in railroad steel and surface waves in mild steel; see [3] for a review. Here we extend those results to the consideration of non-principal waves in deformed steel and nickel, and to pre-strains resulting in turn from the application of a uniaxial stress and of a pure shear stress.

The other counter-intuitive result is that the following statement by Kim and Sachse [3] is not necessarily true: "The principal stress direction is found where the variations of the SAW speeds show symmetry about the direction". Indeed, Tanuma et al. [5] recently showed that for a small-amplitude SAW traveling in the symmetry plane of a transversely isotropic solid, subject to a small pre-strain, the correction to the wave speed due to the pre-stress has sinusoidal variations with respect to the angle of propagation, in line with that statement. Explicitly, Tanuma et al. [5] established the following expression for the correction to the Rayleigh wave speed v_R^0 when the solid is subject to a pre-stress with principal components σ_1, σ_2 in the plane boundary:

$$v_R = v_R^0 + A(\sigma_1 + \sigma_2) + B(\sigma_1 - \sigma_2) \cos 2\psi,$$

where A and B are acousto-elastic coefficients, and ψ is the angle between the direction of propagation and one of the principal directions of pre-stress. However, their result is only true when the pre-stress and accompanying pre-strain are infinitesimal. Here we show that the variations can rapidly lose their sinusoidal regularity beyond that regime, even when a solid is deformed by as little as 1%. Since in non-destructive evaluation and structural health monitoring, the order of magnitude of the pre-stress is not known *a priori*, we conclude that a complete theoretical and numerical investigation needs to be conducted (as here) prior to the determination of the sought-after principal directions. They will not be found simply by measuring the wave speed in all directions until a symmetry in variation is found.

The paper is organized as follows. In the next section we recall the equations governing the propagation of small-amplitude waves in solids subject to a pre-strain of arbitrary magnitude. For the constitutive modeling, we focus on isotropic solids with a strain–energy density expressed as a polynomial expansion up to third order in terms of invariants of the Green strain tensor. Historically, this is the framework in which the equations of *acousto-elasticity* have often been written in considering elastic wave propagation in a slightly pre-deformed, initially isotropic solid. We refer to, for example, [2,3] for an

exposition of the practical and theoretical aspects of this technique, which can be dated back to the early efforts of Brillouin [6] and Hughes and Kelly [4]; see also [7] for a review of acousto-elasticity in solids subject to a general homogeneous pre-strain (not necessarily of infinitesimal amplitude). In Sections 3 and 5, we study body wave and surface wave propagation, respectively (the latter is more complicated than the former, and we thus devote Section 4 to a description of our numerical strategy). For both types of waves we uncover examples of solids (steel, Pyrex glass, polystyrene, nickel, hydrogel with a hard core) where the wave speed does not have its greatest value along the direction of greatest stretch, and/or can be extremal along directions which are *oblique* to the directions of the principal stretches. These counter-intuitive results seem to have gone unnoticed before.

2. Governing equations

2.1. Incremental motions

In this paper, we are concerned with the propagation of small-amplitude waves in deformed materials. The equations governing their motion are now well established. Consider a homogeneous elastic solid, held in a state of static homogeneous deformation, which has brought a material point which was at X in the reference configuration to position $x = x(X, t)$ in the current configuration.

Let (X'_1, X'_2, X'_3) be the coordinates of X with respect to fixed rectangular Cartesian unit basis vectors (e'_1, e'_2, e'_3), and let a pure homogeneous strain be defined by

$$x'_1 = \lambda_1 X'_1, \qquad x'_2 = \lambda_2 X'_2, \qquad x'_3 = \lambda_3 X'_3, \tag{2.1}$$

with respect to the same basis, where the positive constants $\lambda_1, \lambda_2, \lambda_3$ are the *principal stretches* of the deformation. Now consider the material to be a half-space occupying the region $x'_2 \geq 0$ so that the boundary $x'_2 = 0$ is a principal plane of deformation, which we take to be free of traction. Now choose a second set of unit basis vectors (e_1, e_2, e_3), say, with coordinates (x_1, x_2, x_3), so that $x_2 = x'_2$ and the direction of e_1 makes an angle θ with the direction of e'_1. Then

$$\begin{bmatrix} x_1 \\ x_2 \\ x_3 \end{bmatrix} = \begin{bmatrix} \cos\theta & 0 & \sin\theta \\ 0 & 1 & 0 \\ -\sin\theta & 0 & \cos\theta \end{bmatrix} \begin{bmatrix} x'_1 \\ x'_2 \\ x'_3 \end{bmatrix}. \tag{2.2}$$

A small-amplitude wave traveling in this material is described by the associated mechanical displacement field $u = u(x, t)$, satisfying, in the coordinate system (x_1, x_2, x_3), the incremental equations of motion [8],

$$\rho u_{i,tt} = s_{pi,p} = \mathcal{A}_{0piqj} u_{j,pq}, \tag{2.3}$$

where $s_{pi} = \mathcal{A}_{0piqj} u_{j,q}$ are the components of the incremental nominal stress tensor, and $\mathcal{A}_{0piqj}$ are components of the fourth-order tensor of instantaneous moduli $\mathcal{A}_0$ (to be detailed later), a comma followed by an index i (or t) denotes partial differentiation with respect to x_i, $i = 1, 2, 3$, (or t) and ρ is the current mass density. We specialize the analysis to waves that propagate in the x_1 direction, with amplitude variations in the x_2 direction. Hence we seek solutions of the form

$$u = U(x_2)e^{ik(x_1 - vt)}, \tag{2.4}$$

where U, the amplitude, is a function of x_2 only, k is the wavenumber, and v is the wave speed. Then the equations of motion reduce to

$$\mathbf{T}U''(x_2) + ik(\mathbf{R} + \mathbf{R}^{\mathrm{T}})U'(x_2) - k^2(\mathbf{Q} - \rho v^2 \mathbf{I})U(x_2) = \mathbf{0}, \tag{2.5}$$

where the constant tensors $\mathbf{T}, \mathbf{R}, \mathbf{Q}$ are defined in terms of their components with respect to the basis (e_1, e_2, e_3) by

$$T_{ij} = T_{ji} = \mathcal{A}_{02i2j}, \qquad R_{ij} = \mathcal{A}_{02i1j}, \qquad Q_{ij} = Q_{ji} = \mathcal{A}_{01i1j}, \tag{2.6}$$

$\mathbf{I}$ is the identity tensor, and the exponent $^{\mathrm{T}}$ denotes the transpose.

Without loss of generality, we take $\lambda_1 < \lambda_2 < \lambda_3$, so that $\theta = 0°$ corresponds to the direction of greatest compression and $\theta = 90°$ to the direction of greatest stretch. In the coordinate system (x'_1, x'_2, x'_3) aligned with the principal axes of deformation, there are only 15 non-zero components of $\mathcal{A}_0$, given by [8]

$$\begin{aligned}
\mathcal{A}'_{0iijj} &= J^{-1}\lambda_i\lambda_j W_{ij}, \\
\mathcal{A}'_{0ijij} &= J^{-1}(\lambda_i W_i - \lambda_j W_j)\lambda_i^2/(\lambda_i^2 - \lambda_j^2), \quad i \neq j, \lambda_i \neq \lambda_j, \\
\mathcal{A}'_{0ijji} &= J^{-1}(\lambda_j W_i - \lambda_i W_j)\lambda_i\lambda_j/(\lambda_i^2 - \lambda_j^2), \quad i \neq j, \lambda_i \neq \lambda_j, \\
\mathcal{A}'_{0ijij} &= J^{-1}(\lambda_i^2 W_{ii} - \lambda_i\lambda_j W_{ij} + \lambda_i W_i)/2, \quad i \neq j, \lambda_i = \lambda_j, \\
\mathcal{A}'_{0ijji} &= J^{-1}(\lambda_i^2 W_{ii} - \lambda_i\lambda_j W_{ij} - \lambda_i W_i)/2, \quad i \neq j, \lambda_i = \lambda_j,
\end{aligned} \tag{2.7}$$

Table 1
Second- and third-order elastic constants for six different materials.

Material	Units	λ_0	μ_0	A	B	C
Nickel	10^5 bars	7.8	6.12857	−73	−22.5	17.9
Steel	10^5 bars	8.1	5.4	−76	−25	−9
Polystyrene	10^5 bars	0.2889	1.381	−1.00	−0.830	−1.06
Pyrex glass	10^5 bars	2.75	5.583	42	71	−69.6
Hydrogel	NkT	4595	1184	−2737	−1682.5	−3762.5

where $J = \lambda_1 \lambda_2 \lambda_3$ is the dilatation, W is the strain energy density, $W_i = \partial W / \partial \lambda_i$, $W_{ij} = \partial^2 W / \partial \lambda_i \partial \lambda_j$ and there is no sum on repeated indices. In the coordinate system (x_1, x_2, x_3), the components of $\mathcal{A}_0$, required to compute the tensors in (2.6), are given by

$$\mathcal{A}_{0ijkl} = \Omega_{ip} \Omega_{jq} \Omega_{kr} \Omega_{ls} \mathcal{A}'_{0pqrs}, \tag{2.8}$$

where Ω_{ij} is the rotation matrix corresponding to a rotation through the angle θ about $x_2 = x'_2$.

We say that $\mathcal{A}_0$ satisfies the *strong-convexity* condition (S-C) when

$$\mathcal{A}_{0ijkl} \xi_{ij} \xi_{kl} > 0 \quad \text{for all non-zero tensors } \boldsymbol{\xi}, \tag{2.9}$$

but we remark that this condition does not hold in general, only in the region of deformation space corresponding to dead-load stability (see, for example, [8]). The *strong-ellipticity* condition (S-E) reads

$$\mathcal{A}_{0ijkl} n_i n_k m_j m_l > 0 \quad \text{for all non-zero vectors } \boldsymbol{n} \text{ and } \boldsymbol{m}, \tag{2.10}$$

and is implied by strong convexity.

2.2. Deformed materials

For the constitutive modeling of the pre-deformed materials, we focus on general isotropic compressible elastic solids, with a third-order expansion of the strain–energy density in powers of the Green strain tensor **E**, specifically

$$W = \frac{\lambda_0}{2} i_1^2 + \mu_0 i_2 + \frac{A}{3} i_3 + B i_1 i_2 + \frac{C}{3} i_1^3, \tag{2.11}$$

where

$$i_k = \text{tr} \left(\mathbf{E}^k \right) = \frac{1}{2^k} \left[\left(\lambda_1^2 - 1 \right)^k + \left(\lambda_2^2 - 1 \right)^k + \left(\lambda_3^2 - 1 \right)^k \right], \quad k = 1, 2, 3. \tag{2.12}$$

Here, λ_0 and μ_0 are the Lamé coefficients of second-order elasticity and A, B, C are the Landau coefficients of third-order elasticity [9].

For our examples, we use material parameters taken from the literature for nickel [10], steel [10], polystyrene [4], Pyrex glass [10], and a certain hydrogel with a hard core [11], all summarized in Table 1.

We look at two types of pre-deformations: first, that due to a uniaxial stress and second that due to a pure shear stress. A *uniaxial pre-stress* in the $\boldsymbol{e}'_1$ direction is due to a Cauchy stress for which the only non-zero component is $\sigma_{11} = T$, say. It leads to an equibiaxial pre-deformation, with corresponding principal stretches

$$\lambda_1 = \lambda, \qquad \lambda_2 = \lambda_3. \tag{2.13}$$

Here λ is linked to the compressive stress T through the equation $T = J^{-1} \lambda_1 \partial W / \partial \lambda_1$, whilst λ_2 is found in terms of λ by solving

$$0 = \partial W / \partial \lambda_2. \tag{2.14}$$

With our choice (2.11) of strain energy density, this turns out to be a quadratic in λ_2^2.

A *pure shear stress* is applied parallel to the plane of the boundary so that the only non-zero Cauchy stress component is $\sigma_{13} = S$, say. The corresponding pre-deformation is a combination of simple shear in the x_3 direction and a triaxial stretch [12,13]. Here it is a simple exercise to check (see, for example, [10]) that the principal stresses are S, 0, $-S$, and that the corresponding principal directions of stress are along $(1, 0, 1)$, $(0, 1, 0)$, $(1, 0, -1)$, respectively. The principal directions of strain are aligned with these directions, and the principal stretches are found by solving the system

$$S = J^{-1} \lambda_1 \partial W / \partial \lambda_1, \qquad 0 = \partial W / \partial \lambda_2, \qquad -S = J^{-1} \lambda_3 \partial W / \partial \lambda_3, \tag{2.15}$$

for $\lambda_1 = \lambda$, λ_2 and λ_3.

The range of realistic values for λ is restricted by the existence of a solution of the system of Eqs. (2.13) and (2.14) for uniaxial compression, and of the equations in (2.15) for pure shear stress. There is a great variability of this feasible range for λ from one material to another. For example, steel can only be sheared for λ from 1 down to 0.935, below which value there are no real solutions, while for the hydrogel there exists a pure shear stress solution for deformations of up to 40%. We further restrict our range of admissible λ's by assuming that the materials are subject to uniaxial compressive stresses or pure shear stresses only within the region where S and T are monotone functions of λ. This ensures that our results belong to a physically valid regime.
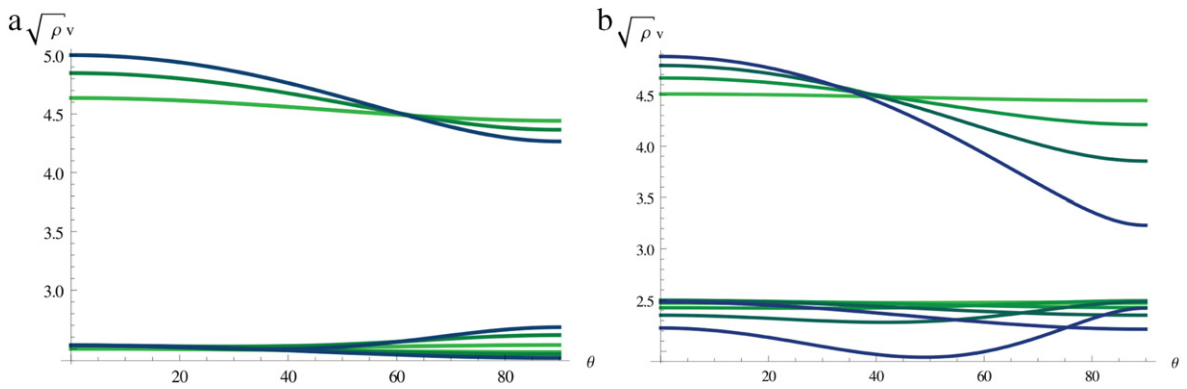
Fig. 2. The three body-wave speed profiles (plotted as $v\sqrt{\rho}$) for nickel under (a) uniaxial compressive stress with principal compression stretch ratio $\lambda = 0.99$ (light green curve), 0.973 (blue–green curve), 0.956 (blue curve); (b) pure shear stress with $\lambda = 0.99$ (light green curve), 0.978 (blue–green curve) and 0.967 (blue curve). (For interpretation of the references to colour in this figure legend, the reader is referred to the web version of this article.)

3. Results for body waves

For homogeneous *body* waves, there are no boundary conditions to satisfy and no amplitude variation to consider. Hence we take

$$\boldsymbol{U}(x_2) = \boldsymbol{U}_0, \tag{3.1}$$

a constant vector, in the governing equation (2.5), resulting in the eigenvalue problem

$$(\mathbf{Q} - \rho v^2 \mathbf{I})\boldsymbol{U}_0 = \mathbf{0}, \tag{3.2}$$

with associated characteristic equation $\det(\mathbf{Q} - \rho v^2 \mathbf{I}) = 0$, a cubic in ρv^2.

For the body waves traveling along the principal direction corresponding to the least principal stretch λ_1, i.e. $\theta = 0°$, we find the three roots

$$\rho v^2 = \mathscr{A}'_{01111}, \ \mathscr{A}'_{01212}, \ \mathscr{A}'_{01313}, \tag{3.3}$$

and similarly for the body waves along the principal direction corresponding to the largest stretch ratio λ_3, i.e. $\theta = 90°$,

$$\rho v^2 = \mathscr{A}'_{03333}, \ \mathscr{A}'_{03131}, \ \mathscr{A}'_{03232}. \tag{3.4}$$

In each set of three roots for ρv^2, the first root corresponds to a pure longitudinal wave and the next two to pure transverse waves.

In general ($\theta \neq 0, 90°$), the characteristic equation factorizes into the product of a term linear in ρv^2 (corresponding to a pure transverse wave polarized along the x_2 direction) and a term quadratic in ρv^2 (with one root corresponding to a pseudo-longitudinal wave and the other to a pseudo-transverse wave); see [14] for details.

Fig. 2 depicts the variations of the three body wave speeds (in this and all subsequent plots it is $v\sqrt{\rho}$ that is plotted) in deformed *nickel* with respect to the angle θ between the direction of greatest compression and the direction of propagation, for different values of compressive stretch under uniaxial and pure shear stresses. The variations of the wave traveling with the intermediate speed meet intuitive expectations: this wave travels at its slowest when $\theta = 0°$ and at its fastest when $\theta = 90°$. However, this scenario is reversed for the fastest and slowest waves, as soon as the solid is deformed: they travel at their fastest along the direction of greatest compression ($\theta = 0°$) and slowest in the orthogonal direction. Moreover, when a pure shear stress induces a compression of more than 3%, we notice that the profile for the slowest body wave develops a new minimum; in effect this wave travels at its slowest in a direction which is *oblique* with respect to the principal directions of strain ($\theta \simeq 50°$).

Fig. 3 shows the corresponding results for deformed *steel*. They are similar to those for deformed nickel, with the difference that the secondary minimum phenomenon occurs under uniaxial compression instead of pure shear stress.

In Figs. 4 and 5, we study body wave propagation in deformed *polystyrene* and *hydrogel*. Here the waves all travel at their fastest along the direction of greatest stretch ($\theta = 90°$) and two of the three waves travel at their slowest in the direction of greatest compression ($\theta = 0°$). There is, however, one wave which travels at its slowest in an oblique direction, for both types of pre-deformations (due to uniaxial stress: figures on the left; due to pure shear stress: figures on the right). They appear at quite large compressions (31% for polystyrene, 39% for hydrogel), which are nonetheless compatible with the soft nature of these solids and with a physically acceptable material response (i.e. the tension and the shear stress are monotone functions of the stretch).

Now we investigate non-principal *surface* wave propagation in a deformed homogeneous half-space. There are several methods of resolution available for these problems; see, for example, [15–18]. Here we adopt a formulation in terms of the surface impedance matrix. In the next section we detail the steps involved in implementing this method, based on the analysis of Fu and Mielke [19].
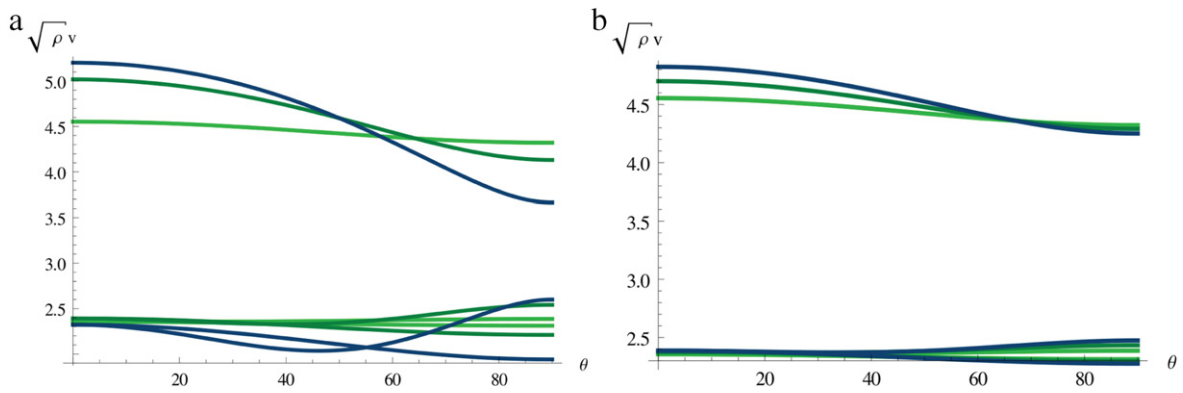
Fig. 3. The three body-wave speed profiles (plotted as $v\sqrt{\rho}$) for steel under (a) uniaxial compressive stress with $\lambda = 0.99$ (light green curve), 0.956 (blue–green curve), 0.922 (blue curve); (b) pure shear stress with $\lambda = 0.99$ (light green curve), 0.981 (blue–green curve), 0.973 (blue curve). (For interpretation of the references to colour in this figure legend, the reader is referred to the web version of this article.)
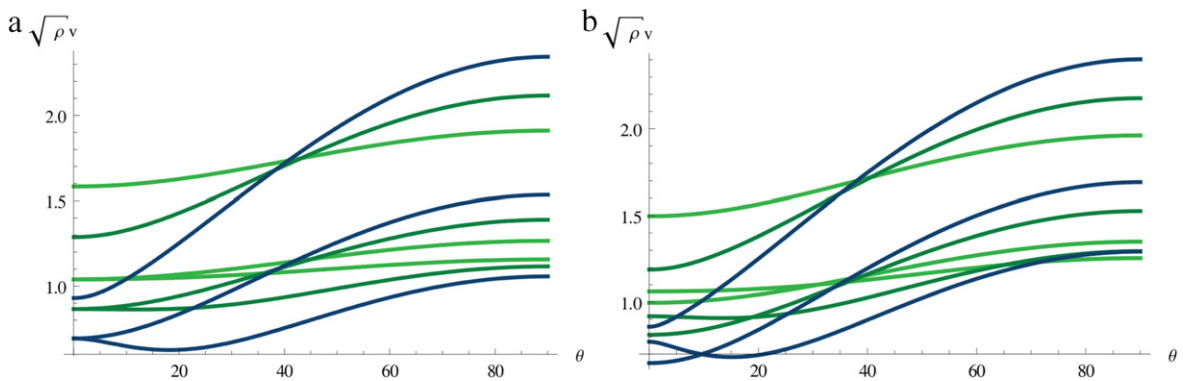
Fig. 4. The three body-wave speed profiles (plotted as $v\sqrt{\rho}$) for polystyrene under (a) uniaxial compressive stress; (b) pure shear stress. The light green curves correspond to $\lambda = 0.91$, the blue–green curves to $\lambda = 0.8$, and the blue curves to $\lambda = 0.69$. (For interpretation of the references to colour in this figure legend, the reader is referred to the web version of this article.)
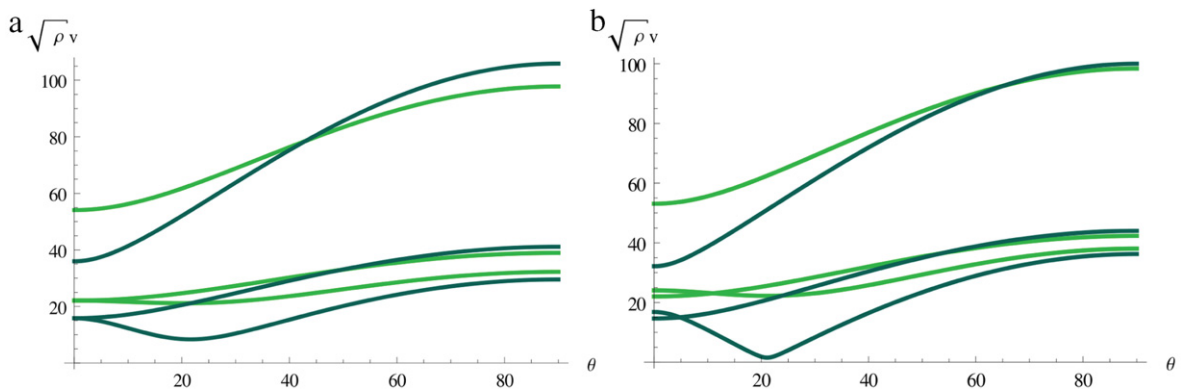
Fig. 5. The three body-wave speed profiles (plotted as $v\sqrt{\rho}$) for hydrogel under (a) uniaxial compressive stress; (b) pure shear stress. The light green curves correspond to $\lambda = 0.75$ (i.e. 25% maximum compression) and the dark green curves to $\lambda = 0.61$ (i.e. 39% maximum compression). (For interpretation of the references to colour in this figure legend, the reader is referred to the web version of this article.)

4. The matrix Riccati method for surface waves

In the following, we replace the tensors **T**, **R**, **Q**, etc., introduced in the previous section by their matrix representations with respect to the Cartesian coordinates (x_1, x_2, x_3). In a nutshell, surface wave propagation is governed by the *algebraic matrix Riccati equation* [20,21,19,22]

$$0 = [Z(v) - iR^T]T^{-1}[Z(v) + iR] - Q + \rho v^2 I, \tag{4.1}$$

the radiation condition,

$$\text{Im Spec } \mathsf{T}^{-1}[i\mathsf{Z}(v) - \mathsf{R}] > 0, \tag{4.2}$$

and the boundary condition of zero incremental traction on $x_2 = 0$, which is equivalent to

$$\det \mathsf{Z}(v) = 0. \tag{4.3}$$

Here, the constant 3×3 matrix $\mathsf{Z}(v)$ is the so-called *surface impedance matrix*. For a given v, $\mathsf{Z}(v)$ is a constant Hermitian matrix, of the form

$$\mathsf{Z} = \begin{bmatrix} Z_1 & Z_4 + iZ_5 & Z_6 - iZ_7 \\ Z_4 - iZ_5 & Z_2 & Z_8 + iZ_9 \\ Z_6 + iZ_7 & Z_8 - iZ_9 & Z_3 \end{bmatrix}, \tag{4.4}$$

say, where the Z_k are real constants ($k = 1, \ldots, 9$). The algebraic matrix Riccati equation (4.1) is itself Hermitian, and thus corresponds to 9 real equations. Coupling it to (4.3) gives a system of 10 equations for the 10 unknowns Z_k and v, and uniqueness of the solution comes from further requiring that $\mathsf{Z}(v)$ be *positive definite*, as discussed below.

The surface impedance matrix $\mathsf{Z}(v)$ in a half-space relates the incremental displacement $\boldsymbol{u}$ to the incremental traction $\boldsymbol{t}$ on the surface $x_2 = \text{constant}$ through the relationship,

$$\boldsymbol{t} = -k\mathsf{Z}(v)\boldsymbol{u}. \tag{4.5}$$

We may rewrite this by noting that the general solution of the homogeneous system of second-order ordinary differential equations with constant coefficients (2.5) for the half-space is of the form $\boldsymbol{U} = e^{ik\mathsf{E}(v)x_2}\boldsymbol{U}_0$, where $\mathsf{E}(v)$ is a constant 3×3 matrix (not to be confused with the Green strain) and $\boldsymbol{U}_0$ is a constant vector. Then the traction is given by

$$t_i = s_{2i} = \mathcal{A}_{02iqj}u_{j,q}, \quad \text{or} \quad \boldsymbol{t} = ik[\mathsf{R} + \mathsf{T}\mathsf{E}(v)]\boldsymbol{u}. \tag{4.6}$$

Now write $\boldsymbol{t} = -ik\boldsymbol{V}e^{i(kx_1-vt)}$, where $\boldsymbol{V} = -[\mathsf{R} + \mathsf{T}\mathsf{E}(v)]\boldsymbol{U}$, so that the impedance relation (4.6) reads

$$\boldsymbol{V} = -i\mathsf{Z}(v)\boldsymbol{U}, \quad \text{with } \mathsf{Z}(v) = -i[\mathsf{R} + \mathsf{T}\mathsf{E}(v)], \tag{4.7}$$

showing that $\mathsf{Z}(v)$ is indeed a constant matrix for a half-space. The matrix $\mathsf{Z}(v)$ corresponding to the existence of a surface wave is the one that satisfies the Riccati equation (4.1), the boundary condition (4.3), and

$$\text{Im Spec } \mathsf{E}(v) > 0,$$

or, equivalently, (4.2). This condition guarantees the correct decay for $\boldsymbol{U}(x_2) = e^{ik\mathsf{E}(v)x_2}\boldsymbol{U}_0$ as x_2 increases with distance away from the free surface.

In the matrix Riccati method, at least two remarkable properties emerge: $\mathsf{Z}(0)$ is positive definite in the region of stability and $\partial\mathsf{Z}(v)/\partial v$ is negative definite as long as $\text{Im Spec } \mathsf{T}^{-1}[i\mathsf{Z}(v) - \mathsf{R}] > 0$. Hence, $\det \mathsf{Z}(v)$ is positive at $v = 0$ and monotonically decreasing as v increases, which means that it is simple to find $\tilde{v}$ numerically such that $\det \mathsf{Z}(\tilde{v}) = 0$. Moreover uniqueness of the surface velocity, calculated by this procedure, is guaranteed. Barnett and Lothe [21], Fu and Mielke [19] and Mielke and Fu [23] have shown these properties, and here we present a somewhat simpler alternative demonstration (see also [24,25] for further impedance formulations).

Recall that the incremental nominal stress has components $s_{pi} = \mathcal{A}_{0piqj}u_{j,q}$ (with respect to the non-principal axes) and that the balance of momentum (2.3) reads

$$\rho u_{i,tt} = s_{pi,p}. \tag{4.8}$$

Now multiply both sides of this by u_i^*, the complex conjugate of u_i:

$$\rho u_i^* u_{i,tt} = u_i^* s_{ji,j} = \left(u_i^* s_{ji}\right)_{,j} - u_{i,j}^* s_{ji} \quad \text{with summation over } i \text{ and } j. \tag{4.9}$$

Then integrate over the region $\mathcal{U} = [x_1, x_1 + \Delta x_1] \times [0, \infty] \times [x_3, x_3 + \Delta x_3]$ in the body, to obtain

$$\int_{\mathcal{U}} \rho u_i^* u_{i,tt} \, dx_1 \, dx_2 \, dx_3 = \int_{\partial\mathcal{U}} u_i^* s_{ji} n_j \, da - \int_{\mathcal{U}} u_{i,j}^* s_{ji} \, dx_1 \, dx_2 \, dx_3, \tag{4.10}$$

where $\boldsymbol{n}$ is the outward unit normal vector to the boundary $\partial\mathcal{U}$ and da the associated area element. Now substitute $\boldsymbol{u}(x_1, x_2, x_3) = \boldsymbol{U}(x_2)e^{ik(x_1-vt)}$ to arrive at[1]

$$-k^2 v^2 \int_0^\infty \rho \, \boldsymbol{U}^*(y) \cdot \boldsymbol{U}(y) \, dy = u_i^* t_i \, |_{y=0}^{y=\infty} - \int_0^\infty \mathcal{A}_{0jilk} u_{i,j}^* u_{k,l} \, dy, \tag{4.11}$$

---

[1] Here and in the following we write the scalar product of two vectors as $\boldsymbol{a} \cdot \boldsymbol{b}$ rather than in the matrix form $\boldsymbol{a}^\mathsf{T}\boldsymbol{b}$.

where we have introduced the components t_i, defined in (4.6), of the traction $\boldsymbol{t}$ on planes normal to the x_2-axis. Observe that the above equation is independent of x_1 and x_3. Finally, assume that the wave amplitude decays away from the free surface, so that $\boldsymbol{U}(\infty) = \boldsymbol{0}$. Then substitute for t_i from (4.5) and rearrange to obtain

$$k\,\boldsymbol{U}^*(0) \cdot \mathsf{Z}(v)\boldsymbol{U}(0) = \int_0^\infty \mathcal{A}_{0jilk} u_{i,j}^* u_{k,l}\, dx_2 - k^2 v^2 \int_0^\infty \rho\, \boldsymbol{U}^*(x_2) \cdot \boldsymbol{U}(x_2)\, dx_2. \tag{4.12}$$

Here, only Z depends on v because (i) $\boldsymbol{U}$ can be chosen independently of v since for any choice of displacement field $\boldsymbol{U}$, a traction field $\boldsymbol{V}$ can be determined by Eq. (4.7) such that momentum is balanced, and (ii) v cancels out in the products $u_{i,j}^* u_{l,k}$. Therefore, by differentiating with respect to v, we obtain

$$\boldsymbol{U}^*(0) \cdot \frac{d\mathsf{Z}(v)}{dv} \boldsymbol{U}(0) = -2kv \int_0^\infty \rho\, \boldsymbol{U}^*(x_2) \cdot \boldsymbol{U}(x_2)\, dx_2 < 0, \tag{4.13}$$

while writing Eq. (4.12) at $v = 0$ gives

$$k\,\boldsymbol{U}^*(0) \cdot \mathsf{Z}(0)\boldsymbol{U}(0) = \int_0^\infty \mathcal{A}_{0jilk} u_{i,j}^* u_{k,l}\, dx_2, \tag{4.14}$$

for any choice of $\boldsymbol{U}(0)$. Clearly $d\mathsf{Z}/dv$ is negative definite by (4.13) and, from the strong-convexity condition (2.9) and (4.14), $\mathsf{Z}(0)$ is positive definite if at least one of the components of $u_{i,j}$ is non-zero. Below we show that $\mathsf{Z}(0)$ is positive definite when the deformation is within the region of (dead-load) stability.

For a *material in the reference configuration*, strong convexity is considered to be a necessary physical requirement, and it implies that $\mathsf{Z}(0)$ is positive definite and that the decay condition (4.2) holds at $v = 0$. For a *pre-stressed material*, strong convexity is not expected in general. However, $\mathsf{Z}(0)$ is positive definite for a deformation in the region of dead-load stability. Let the magnitude of the finite deformation be parameterized by α, with $\alpha = 0$ corresponding to no deformation (for instance, α can be the amount of shear in a simple shear pre-deformation, or the elongation $\lambda - 1$ in a uniaxial stretch). Then the surface-impedance Z depends on α as well as on v and the boundary condition of no incremental surface-traction (the secular equation) takes the form

$$\det \mathsf{Z}(v, \alpha) = 0. \tag{4.15}$$

Assume that for $\alpha = 0$ the strong-convexity condition (2.9) is satisfied, so that $\mathsf{Z}(0, 0)$ is positive definite. As α is increased and the deformation moves into the region of dead-load stability, consider the change in the eigenvalues of $\mathsf{Z}(0, \alpha)$; these eigenvalues are positive until α reaches a critical value α^*, say, when at least one eigenvalue becomes zero and $\det \mathsf{Z}(0, \alpha^*) = 0$. At this point the half-space supports a standing-wave solution given by (2.4) with $v = 0$ (at the boundary of the dead-load stability region), and the material has buckled (that is, it is unstable, at least in the linearized sense). For waves along the principal direction, this buckling criterion can be shown to be the same as found in [26]. For $\alpha > \alpha^*$ we say that the half-space is unstable with respect to surface-wave perturbations [19].

We are only interested in surface waves in the stable region $0 < \alpha < \alpha^*$ where $\mathsf{Z}(0, \alpha)$ is positive definite, and we define an implicit curve $v \mapsto \mathsf{Z}(v, \alpha)$ by using the Riccati equation (4.1). As long as $\operatorname{Im} \operatorname{Spec} \mathsf{T}^{-1}(i\mathsf{Z}(v, \alpha) - \mathsf{R}) > 0$ holds, we increase v until $\det \mathsf{Z}(v, \alpha) = 0$. If along this curve $\operatorname{Im} \operatorname{Spec} \mathsf{T}^{-1}(i\mathsf{Z}(v, \alpha) - \mathsf{R}) \leq 0$ before $\det \mathsf{Z}(v, \alpha)$ reaches zero, then there is no surface-wave.
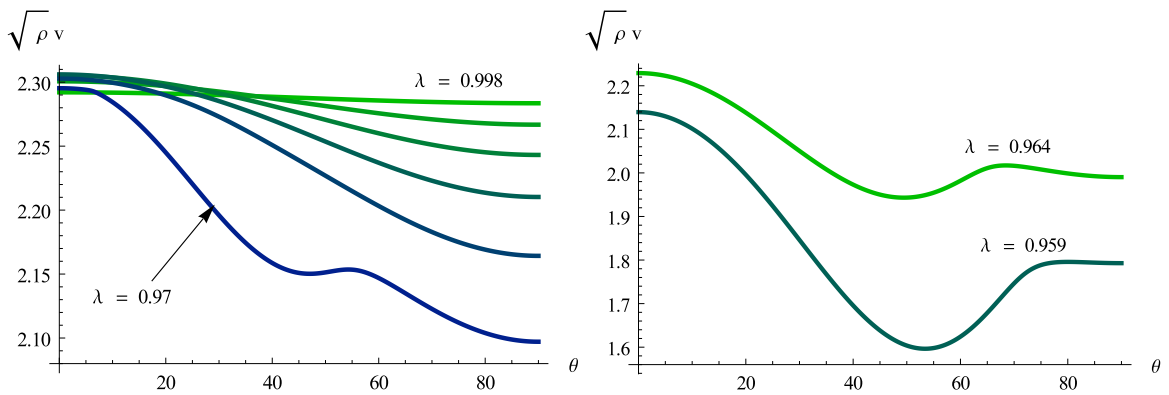
5. Results for surface waves

We transform the above analysis into a numerical method by choosing $\mathcal{A}_0$ for which there is a positive definite $\mathsf{Z}(0)$ satisfying Eq. (4.1). Then, as v is increased, we calculate the implicit curve for $\mathsf{Z}(v)$ from $\mathsf{Z}(0)$ up to $\mathsf{Z}(\hat{v})$ where $\det \mathsf{Z}(\hat{v}) = 0$, all the while verifying that $\operatorname{Im} \operatorname{Spec} \mathsf{T}^{-1}(i\mathsf{Z} - \mathsf{R}) > 0$. From that point on, we calculate another implicit curve that satisfies Eqs. (4.1) and (4.3) by varying $\mathcal{A}_0$ (for instance, by varying the angle of propagation with respect to the principal axes or by varying the amplitude of the pre-deformation). If at some point $\operatorname{Im} \operatorname{Spec} \mathsf{T}^{-1}(i\mathsf{Z} - \mathsf{R}) \leq 0$, then to confirm that there is no surface-wave calculate the implicit curve for $v \mapsto \mathsf{Z}(v)$ that departs from $\mathsf{Z}(0)$ and if, for some v, $\operatorname{Im} \operatorname{Spec} \mathsf{T}^{-1}(i\mathsf{Z}(v) - \mathsf{R}) \leq 0$, then no surface-wave exists; if not, then varying $\mathcal{A}_0$ has caused a discontinuous jump in the velocity, which may indeed be possible.

Using this method we now present Surface Acoustic Wave (SAW) velocity profiles in several materials subject to either a uniaxial compressive stress or a pure shear stress, applied in the plane parallel to the free surface $x_2 = 0$.

Fig. 6 depicts the variations of the surface wave speed with the angle of propagation with respect to the principal directions of strain in *nickel* subject to a uniaxial compressive stress. In the early stages of compression, from 1% to 3% compressive stretch say, "the variations of the SAW speeds show symmetry about the [principal] direction[s]" as stated by Kim and Sachse [3], with the proviso that the SAW travels at its fastest along the direction of greatest compression $\theta = 0°$ and at its slowest along the direction of greatest stretch $\theta = 90°$ (in line with the behavior of the body waves in nickel, as shown in the previous section). However, as the material is further compressed (compression beyond 10%), secondary extrema develop:
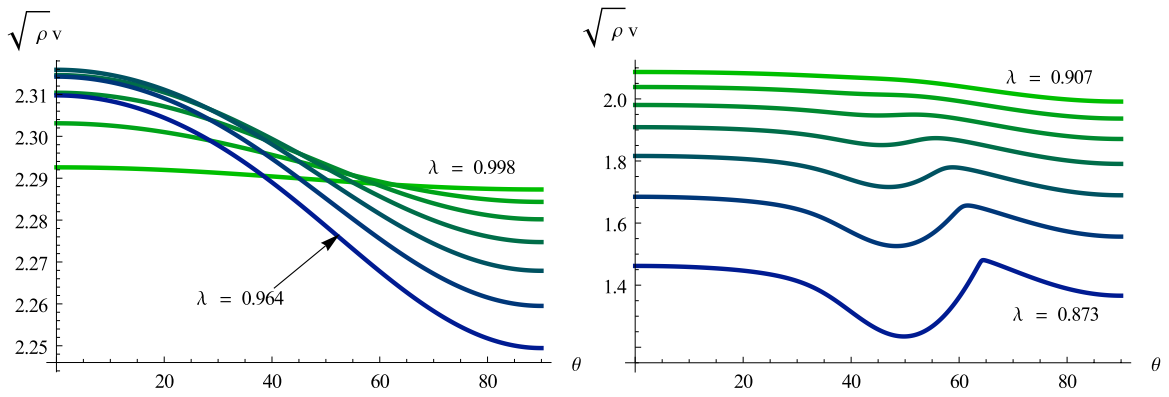
Fig. 6. Speed profiles for surface waves (plotted as $v\sqrt{\rho}$) in nickel subject to uniaxial compressive stress, with pre-stretch λ decreasing from 0.998 to 0.964 (on the left) and from 0.907 to 0.873 (on the right). As the color of the curves changes from green to blue, λ is decreased by regular increments of 0.0057 from one curve to the next. (For interpretation of the references to colour in this figure legend, the reader is referred to the web version of this article.)
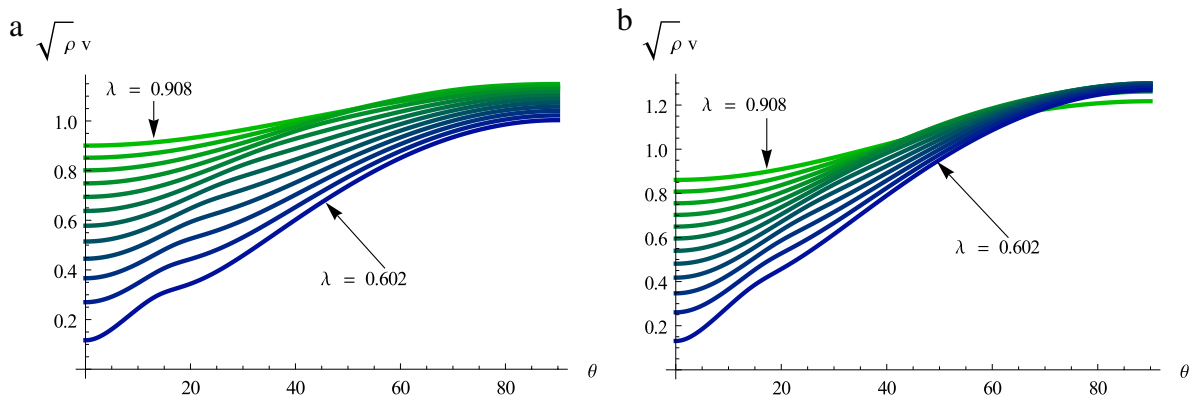

Fig. 7. Speed profiles for surface waves (plotted as $v\sqrt{\rho}$) in nickel subject to pure shear stress, with pre-stretch λ decreasing from 0.998 to 0.970 (on the left) and from 0.964 to 0.959 (on the right). As the color of the curves changes from green to blue, λ is decreased by regular increments of 0.0057 from one curve to the next. (For interpretation of the references to colour in this figure legend, the reader is referred to the web version of this article.)
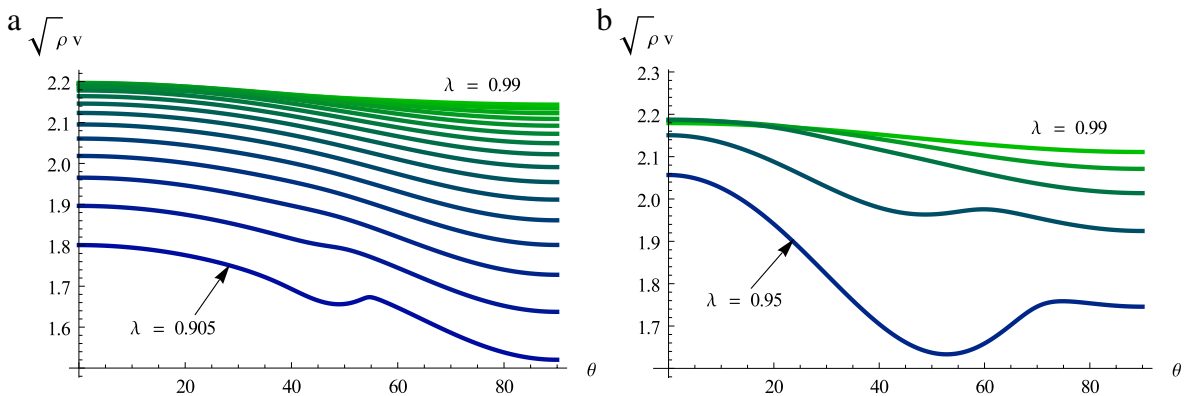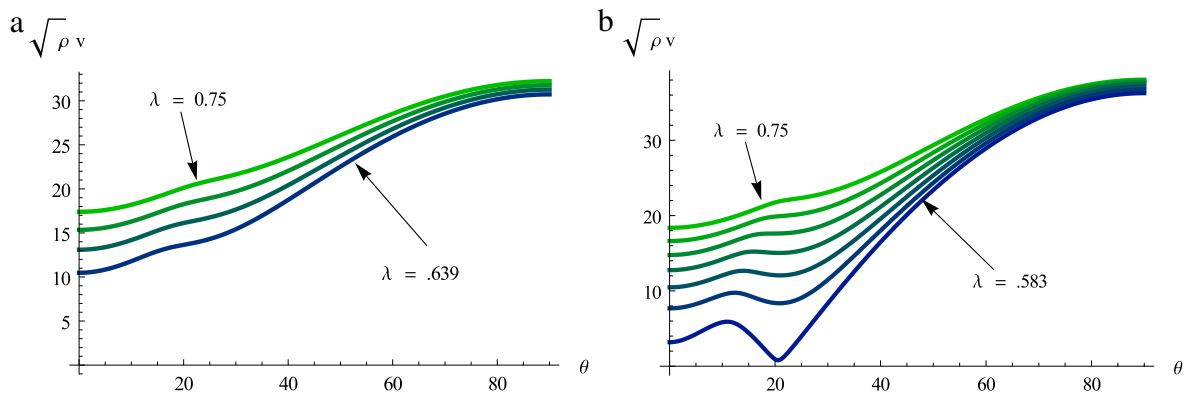

Fig. 8. Speed profiles for surface waves (plotted as $v\sqrt{\rho}$) in steel subject to (a) uniaxial compressive stress, with pre-stretch λ decreasing from 0.990 to 0.905 (on the left) and (b) pure shear stress, with pre-stretch λ decreasing from 0.99 to 0.95 (on the right). As the color of the curves changes from green to blue, λ is decreased by regular increments of 0.0056 from one curve to the next. (For interpretation of the references to colour in this figure legend, the reader is referred to the web version of this article.)

for $\lambda \geq 0.895$, the fastest SAW travels in the $\theta \simeq 65°$ direction and the slowest SAW travels in the $\theta \simeq 45°$ direction. A similar phenomenon occurs when nickel is subject to a pure shear stress, as shown in Fig. 7: then the slowest wave travels at the oblique angle $\theta \simeq 50°$ when the material is compressed by as little as 3.6%; see figure on the right.

For deformed *steel*, we observe similar characteristics for the SAW velocity profile under uniaxial compression and pure shear stress as for deformed nickel, as shown in Fig. 8. *Pyrex glass* also exhibits a local minimum under pure shear stress,

Fig. 9. Speed profiles for surface waves (plotted as $v\sqrt{\rho}$) in polystyrene subject for (a) uniaxial compressive stress, with pre-stretch λ decreasing from 0.908 to 0.602 (on the left) and (b) pure shear stress, with pre-stretch λ decreasing from 0.908 to 0.602 (on the right). As the color of the curves changes from green to blue, λ is decreased by regular increments of 0.028 from one curve to the next. (For interpretation of the references to colour in this figure legend, the reader is referred to the web version of this article.)

Fig. 10. Speed profiles for surface waves (plotted as $v\sqrt{\rho}$) in hydrogel subject to (a) uniaxial compressive stress, with pre-stretch λ decreasing from 0.750 to 0.639 (on the left) and (b) pure shear stress, with pre-stretch λ decreasing from 0.750 to 0.583 (on the right). As the color of the curves changes from green to blue, λ is decreased by regular increments of 0.028 from one curve to the next. (For interpretation of the references to colour in this figure legend, the reader is referred to the web version of this article.)

when $\lambda \simeq 0.975$, which then becomes a global minimum when $\lambda = 0.97$, i.e. under a compression of 3% (figures not shown to save space).

SAWs in deformed *polystyrene* behave in a more orderly way, as they travel at their fastest along the direction of greatest stretch $\theta = 90°$ and at their slowest along $\theta = 0°$ (see Fig. 9). Although the first derivative of the velocity profile is not a monotone function of the angle, no secondary extremum develops, in contrast to the behavior of the body waves in the same material (see previous section).

Finally, SAW propagation in deformed *hydrogel* is also almost regular under uniaxial compression even at a relatively large strain (up to 40%); see Fig. 10(a). However, two secondary extrema develop under pure shear stress, with the secondary minimum in an oblique direction, eventually becoming an absolute minimum; see Fig. 10(b).

6. Conclusion

Clearly, the existence of oblique slowest waves greatly complicates the determination of the principal directions of strain in a deformed body. Finding the direction where a wave travels at its slowest or fastest is not a guarantee of having determined the direction of greatest compression or tension, or that it is indeed a principal direction. In our examples, we have found that the slowest body wave can sometimes be along an oblique direction and similarly for surface waves. However, we found that the fastest body waves do indeed travel along a principal direction, a criterion which can thus be used to determine principal directions, at least in deformed nickel, steel, polystyrene and hydrogel. Unfortunately, this characteristic does not carry over to the case of surface waves, as the example of nickel subject to pure shear stress shows, where the fastest surface wave is oblique. The overall conclusion is that, for a given solid, a full analysis of wave speed variation with angle of propagation, such as that conducted in this paper, is required.

Acknowledgments

References

[1] R.A. Guyer, P.A. Johnson, Nonlinear Mesoscopic Elasticity, Wiley-VCH, Weinheim, 2009.
[2] Y.-H. Pao, W. Sachse, H. Fukuoka, Acoustoelasticity and ultrasonic measurements of residual stresses, in: W.P. Mason, R.N. Thurston (Eds.), Physical Acoustics, Vol. 17, Academic Press, 1984, pp. 61–143.
[3] K.Y. Kim, W. Sachse, Acoustoelasticity of elastic solids, in: Levy, Bass, Stern (Eds.), Handbook of Elastic Properties of Solids, Liquids, and Gases, Vol. 1, Academic Press, New York, 2001, pp. 441–468.
[4] D.S. Hughes, J.L. Kelly, Second-order elastic deformation of solids, Phys. Rev. 92 (1953) 1145–1149.
[5] K. Tanuma, C.-S. Man, W. Du, Perturbation of phase velocity of Rayleigh waves in pre-stressed anisotropic media with orthorhombic principal part, Math. Mech. Solids. http://dx.doi.org/10.1177/1081286512438882 (in press).
[6] L. Brillouin, Sur les tensions de radiation, Ann. Phys. Ser. 10 4 (1925) 528–586.
[7] M. Destrade, R.W. Ogden, On stress-dependent elastic moduli and wave speeds, IMA J. Appl. Math. http://dx.doi.org/10.1093/imamat/hxs003 (in press).
[8] R.W. Ogden, Nonlinear Elastic Deformations, Dover, New York, 1997.
[9] L.D. Landau, E.M. Lifshitz, Theory of Elasticity, third ed., Pergamon, New York, 1986.
[10] A.I. Lurie, Theory of Elasticity, Springer, Berlin, 2005.
[11] M.S. Wu, H.O.K. Kirchner, Nonlinear elasticity modeling of biogels, J. Mech. Phys. Solids 58 (2010) 300–310.
[12] L.A. Mihai, A. Goriely, Positive or negative poynting effect? The role of adscititious inequalities in hyperelastic materials, Proc. R. Soc. Lond. Ser. A 467 (2011) 3633–3646.
[13] M. Destrade, J.G. Murphy, G. Saccomandi, Simple shear is not so simple, Int. J. Non-Linear Mech. 47 (2012) 210–214.
[14] A.N. Norris, Propagation of plane waves in a pre-stressed elastic medium, J. Acoust. Soc. Am. 74 (1983) 1642–1643.
[15] G.A. Rogerson, K.J. Sandiford, Harmonic wave propagation along a non-principal direction in a pre-stressed elastic plate, Internat. J. Engrg. Sci. 37 (1999) 1663–1691.
[16] M. Destrade, M. Ottenio, A.V. Pichugin, G.A. Rogerson, Non-principal surface waves in deformed incompressible materials, Internat. J. Engrg. Sci. 42 (2005) 1092–1106.
[17] P. Kayestha, A.C. Wijeyewickrema, K. Kishimoto, Wave propagation along a non-principal direction in a compressible pre-stressed elastic layer, Int. J. Solids Struct. 48 (2011) 2141–2153.
[18] N. Gandhi, J.E. Michaels, S.J. Lee, Acoustoelastic Lamb wave propagation in biaxially stressed plates, J. Acoust. Soc. Am. 132 (2012) 1284–1293.
[19] Y.B. Fu, A. Mielke, A new identity for the surface impedance matrix and its application to the determination of surface-wave speeds, Proc. Roy. Soc. Lond. A 458 (2002) 2523–2543.
[20] S.V. Biryukov, Impedance method in the theory of elastic surface waves, Sov. Phys. Acoust. 31 (1985) 350–354.
[21] D.M. Barnett, J. Lothe, Free surface (Rayleigh) waves in anisotropic elastic half-spaces: the surface impedance method, Proc. Roy. Soc. Lond. A 402 (1985) 135–152.
[22] A.N. Norris, A.L. Shuvalov, Wave impedance matrices for cylindrically anisotropic radially inhomogeneous elastic solids, Q. J. Mech. Appl. Math. 63 (2010) 401–435.
[23] A. Mielke, Y.B. Fu, A proof of uniqueness of surface waves that is independent of the stroh formalism, Math. Mech. Solids 9 (2003) 5–15.
[24] A.L. Shuvalov, O. Poncelet, M. Deschamps, General formalism for plane guided waves in transversely inhomogeneous anisotropic plates, Wave Motion 40 (2004) 413–426.
[25] V.I. Alshits, G.A. Maugin, Dynamics of multilayers: elastic waves in an anisotropic graded or stratified plate, Wave Motion 41 (2005) 357–394.
[26] M.A. Dowaikh, R.W. Ogden, On surface waves and deformations in a compressible elastic half-space, Stab. Appl. Anal. Cont. Media 1 (1991) 27–45.